Available online at www.sciencedirect.com
SCIENCE DIRECT
Journal of Magnetic Resonance 181 (2006) 244–253
JMR Journal of Magnetic Resonance
www.elsevier.com/locate/jmr

Cogwheel phase cycling in common triple resonance NMR experiments for the liquid phase

Gerhard Zuckerstätter, Norbert Müller *

Institute of Organic Chemistry, Johannes Kepler University, Altenbergerstrasse 69, A-4040 Linz, Austria

Received 2 February 2006; revised 22 April 2006
Available online 6 June 2006

Abstract

We demonstrate that cogwheel phase cycling, which was previously only used in solid state NMR, can be applied to optimize the efficiency of commonly used pulse sequences in multiple resonance liquid-state biomolecular NMR. In favorable cases the required minimum number of scans can be reduced by more than 80% as compared to a corresponding sequence with nested phase cycles. Since cogwheel phase cycling procedures can be designed for a range of scan numbers, and can be combined with pulsed field gradients, the total experiment time can be adjusted closely to the required signal-to-noise ratio with minimal overhead. Examples are shown for 3D-TROSY-HNCO, 3D-TROSY-HNCACO, and 3D-HACACO experiments on diamagnetic and paramagnetic proteins.

Keywords: Cogwheel phase cycling; Triple resonance; Coherence selection; Accelerated acquisition; Protein structure determination; TROSY

1. Introduction

The time requirements for multi-dimensional NMR-experiments present a significant bottle-neck for many structure and dynamics oriented research efforts. Therefore implementation of time-saving NMR methods has become a major target of pulse sequence development. The total time necessary for a particular NMR experiment is not only determined by the need to achieve a sufficient signal-to-noise ratio (SNR). Often the number of repetition cycles for suppressing unwanted signals as well as the resolution requirements for indirectly sampled evolution dimensions of multi-dimensional experiments increase the duration of experiments tremendously beyond the amount required to achieve sufficient signal-to-noise ratios. Because of recent improvements of the sensitivity of NMR spectrometers, e.g. through high performance low-noise electronic circuits and cryogenically cooled probes and preamplifiers [1,2], in many cases signal-to-noise ratio requirements are no longer determining the low limit of the total transient numbers. A number of different approaches that allow for more efficient acquisition of multi-dimensional NMR spectra have been published recently. Single scan multi-dimensional spectroscopy probably yields the most radical improvement [3–5]. But it poses some stringent hardware requirements, which make implementation still difficult for routine use. Highly optimized pulse schemes allow for extremely fast repetition intervals, but are limited to some HSQC-type experiments and particular relaxation regimes [6]. Approaches involving reduced dimensionality [7,8] and projection–reconstruction [9–12] can be readily implemented for most known multi-dimensional experiments using current hardware. These techniques reduce the number of data points required in the evolution dimensions and can be combined with any coherence selection approach. Levitt and co-workers have introduced cogwheel phase cycling and achieved very significant reductions of the number of phase cycle steps in solid state NMR

* Corresponding author. Fax: +43 732 2468 8747.
E-mail address: norbert.mueller@jku.at (N. Müller).

1090-7807/$ - see front matter © 2006 Elsevier Inc. All rights reserved.
doi:10.1016/j.jmr.2006.05.004

experiments [13–15]. Here we present first results on the application of cogwheel phase cycling in 3D triple resonance experiments on proteins, which are easily generalized for other liquid-state multi-pulse experiments.

Selection of the appropriate coherence transfer pathways (CTPs) [16] is essential in virtually any NMR pulse sequence in order to suppress undesired signals in the spectrum, particularly for multi-dimensional experiments. Three fundamental approaches for coherence selection in NMR exist: Phase cycling [17,16], pulsed B_o-field gradients (PFGs) [18,19], and pulsed radio-frequency (rf)-gradients [20]. While the last mentioned approach is not widely used today, both phase cycles and PFGs are integral to most routinely used multiple-pulse and multi-dimensional NMR techniques, in particular to those essential for NMR of biological macromolecules.

By using PFGs one can, in principle, achieve coherence selection in a single pass of a pulse sequence. However, inherent limitations prevent the exclusive use of pulsed magnetic field gradients for coherence selection. First, PFGs introduce additional delays, which often require additional refocusing pulses and delays for compensation of coherent evolution during these periods. Second, when applied during evolution periods, PFGs also lead to a loss of total amplitude, since parallel CTPs can usually not be selected by PFGs. In addition, in fast relaxing systems like paramagnetic proteins [21,22] the delays associated with gradients may cause significant signal attenuation. Application of PFGs may also compromise the spectrum quality because of Eddy currents and fluctuations in the spectrometer's field stabilization circuits (lock-system). In most pulse sequences used today and as supplied in most instrument manufacturers' libraries, phase cycles and PFGs are usually combined to achieve the desired coherence selections. Phase cycling is implemented almost exclusively in the form of so-called "nested" phase cycles (nPCs). As outlined in the following section the number of steps in nested phase cycles increases exponentially with the number of pulses that are cycled. As a consequence frequently a compromise between optimum coherence selectivity and duration of an experiment must be found.

The work presented here has two main objectives: (1) to assess the potential and limitations of cogwheel phase cycles in liquid-state NMR and (2) to introduce time saving cogwheel phase cycles for some commonly used liquid-state triple resonance 3D pulse sequences, which can be easily generalized for other experiments.

2. Theory

Phase cycling in an NMR pulse sequence eliminates signals from the spectra by addition and subtraction of individual free induction decays, based on their differential response to the variation of the pulses' rf-phases. The causes of such unwanted signals may be artefacts from spectrometer electronics, pulse-imperfections or -calibration deficiencies, signals from undesired coherences or NMR response from certain chemical species in the sample, e.g. the solvent. The basic condition describing the constructive interference governing the coherence selection process by phase cycling is

$$\sum_i \Delta p_i \phi_i = -\rho. \tag{1}$$

Here, Δp_i is the (desired) change of coherence order effected by the pulse or pulse group i; ϕ_i is the rf-phase of i, and ρ is the receiver reference phase. In "classical" or "nested" phase cycling [17,16] the phases of different pulses in a particular sequence are cycled independently from each other. That means, the phase of each pulse or pulse group k is incremented systematically through a full circle, while the phases $\phi_{i\neq k}$ are kept constant and ρ is set in each step according to Eq. (1). This incrementation scheme is repeated for all relevant pulses or pulse groups of a pulse sequence. Therefore, the total number of steps in an nPC is the product of all individual cycle lengths, which increases approximately exponentially with the number of cycled pulses. In a cogwheel phase cycle (cPC) [13–15] all pertinent pulse phases are incremented simultaneously, while the receiver phase is adjusted following Eq. (1). To describe the synchronous phase incrementation, each cycled pulse i is assigned a winding number v_i. Thus the phase of a pulse i in the m^{th} step of a cPC is given by

$$\phi_i^{(m)} = \frac{2\pi v_i}{N} m. \tag{2}$$

Here, N is the total number of steps in a cPC. As Levitt et al. [14] have shown, this number grows much slower with the number of phase cycled pulses for a particular coherence pathway than the total number of steps in an nPC. The receiver reference phase $\phi_{rec}^{(m)}$ then follows an equation analogous to Eq. (2), with a winding number v_{rec}. Here, we will use the systematic nomenclature for cPCs that was introduced in Ref. 14: COG $N(v_1, v_2, v_3, \ldots v_n; v_{rec})$ describes an N step cogwheel phase cycle, with winding numbers $v_1, v_2, v_3, \ldots v_n$ for the pulses or pulse groups 1 to n, and a receiver phase winding number of v_{rec}.

While the design of nPCs is rule based and, with a little experience, can be done "by hand", cPCs require systematic numerical searches through the multi-dimensional space of pulse winding numbers to find combinations fulfilling Eq. (1) for a particular CTP.

3. Methods

For the analysis of coherence transfer pathways the program CCCP [24] developed earlier in our lab was used. It computes and displays the amplitudes and phases of individual coherence pathways in pulse sequences taking into account PFGs and phase cycles. Deliberately pulse angles miss-set by −5% were used in these calculations to mimic the situation of real NMR experiments, where rf-offset and -inhomogeneities are present. The program CCCP++ by Jerschow and Kumar [25], which is based on an

extension of the CCCP algorithms, was used to search for cPCs. For one particular coherence pathway multiple cPC solutions are usually obtained. These may differ in their actual ability to suppress undesired pathways. Therefore, each set of cPCs found was further analyzed by comparing the relative amplitudes of positively selected versus the ones of undesired coherence pathways.

It should be noted that the computational requirements in time and memory of both programs (CCCP [24] and CCCP++ [25]) increase super-exponentially with increasing numbers of pulses and spins. Therefore, we made some simplifying assumptions without restricting the general validity of the results: The proton channel was omitted in the displayed CCCP calculations, since none of the proton pulses were phase cycled. This is justified by the fact that practical experience has shown that optimum solvent (water) signal suppression in the type of experiments investigated here, can only be achieved, if the relative proton pulse phases are optimized and remain unchanged during accumulation. Since CCCP implies -1 quantum coherence (-1 QC) at the end of every pulse sequence on the acquisition channel, omitting the proton channel required the introduction of a dummy pulse (not existing in the real pulse sequence) to convert one heteronucleus' coherence order from 0 to -1 QC. Additional acceleration of the computations was achieved by restricting the homonuclear coherence orders to $-2 \leqslant p \leqslant 2$, except for the ^{15}N channel, where $-1 \leqslant p \leqslant 1$ was used. This is justified by the absence of significant homonuclear ^{15}N couplings in the target spin systems, proteins. Also by assuming pure z-magnetization as an initial condition, the simulations could be restricted to coherence orders $-1 \leqslant p \leqslant 1$ in the free precession period following first pulse in any sequence.

Experimental details are given in the respective figure captions.

4. Computational results

4.1. TROSY-HNCO, -HNCA, and -HN(CA)CO

We chose to investigate commonly used TROSY-type pulse sequences, since they are most important in high field NMR. Also due to the absence of broadband decoupling and its associated heating problems the results can be quantified more reliably. For three different triple resonance 3D NMR pulse sequences, TROSY-HNCO, TROSY-HNCA, and TROSY-HN(CA)CO, cogwheel phase cycles were generated and analyzed as described in the previous Section. The cPCs found apply both for the two- and three-dimensional versions of the experiments.

First, we compare nested and cogwheel phase cycling schemes for two commonly used TROSY-HNCO pulse sequences. The experiment described by Salzmann et al. [23] is implemented with minor modifications in the Bruker pulse sequence library [26] and is displayed in Fig. 1A. Another frequently used implementation of TROSY-HNCO as described by Yang and Kay [33] is displayed in Fig. 2A. The latter sequence demands modifications of pulse phase settings to obtain a spectrum on Bruker DRX spectrometers. The adaptions are described in the figure caption of Fig. 2. Both experiments employ PFGs for compensation of imperfect proton refocusing pulses, which thus do not cause additional delays. Further PFGs are used in the Bruker library implementation during the WATERGATE [28] solvent suppression and in Ref. [33] for echo/anti-echo selection. Both pulse sequences use slightly different eight-step nPC schemes. Since the same coherence pathways are selected in both pulse sequences identical phase cycling schemes can be used. Accordingly, both original nested phase cycles can be replaced by the same cPC, as is shown later. With this in mind, the following computational results refer to the pulse sequence of Salzmann et al. [23]. The original eight-step nPC procedure uses four steps on the 90° pulse (6 in Fig. 1A) preceding the t_2 (^{15}N) evolution time and independently alternates the 90° pulse (10 in Fig. 1A) before the t_1 (^{13}C=O) evolution time. Quadrature detection is achieved by echo/anti-echo ($p = \pm 1$) selection on alternate increments [29] during t_2, and by States-TPPI [30] phase incrementation in t_1, allowing both the echo and anti-echo pathways to pass in parallel. Parallel coherence pathways are rarely found in cPC schemes [14]. In this particular case, however, we found COG*4* and COG*6* schemes, which by cycling the same two pulses as the nPC also select the same parallel coherence pathways. Thus no per scan signal-amplitude is lost. All cPCs retaining parallel coherence pathways cycle pulse 6 (Fig. 1A) with a winding number of $N/2$, which yields a 180° phase increment like in the ''nested'' case. This appears to be a requirement for the selection of parallel coherence pathways. All solutions for odd N (3, 5, or 7), which cycle two pulses, select only a single coherence pathway for the t_1 evolution time. Accordingly, half of the intensity is lost as compared to schemes with even N. The only odd N COGN solutions found, which allow for parallel pathways, are not real cogwheel phase cycles since only one $v \neq 0$, i.e. only one pulse is cycled. The 90° pulse 10 (Fig. 1A) preceding the t_2 (^{15}N) evolution time is cycled with winding numbers v or $-v$ to select the echo- or anti-echo-pathway, respectively. This suggests a cogwheel phase cycle design rule: by inverting winding number modulo N symmetrical pathways around $p = 0$ are selected.

The CCCP [24] coherence transfer diagrams of the phase cycles, which select parallel pathways, exhibit only minor differences (Fig. 1B). The COG*6*(3,1;2) phase cycle (N.B.: the winding numbers refer to the only cycled pulses 6 and 10 (Fig. 1A), and the receiver phase, respectively) selects parallel pathways $0 \rightarrow \pm 1$ on pulse 6 (v_1) and simultaneously only the echo pathway $0 \rightarrow +1$ on pulse 10 (v_2). To obtain the corresponding anti-echo pathway for t_2, the second pulse winding numbers must be inverted (modulo N), yielding COG*6*(3,5;2). To indicate the different winding numbers for the echo and anti-echo pathways in cPCs we will use v_e/v_a, i.e. COG*6*(3,1/5;2) in this case. Table 1 lists the phases for the phase cycling

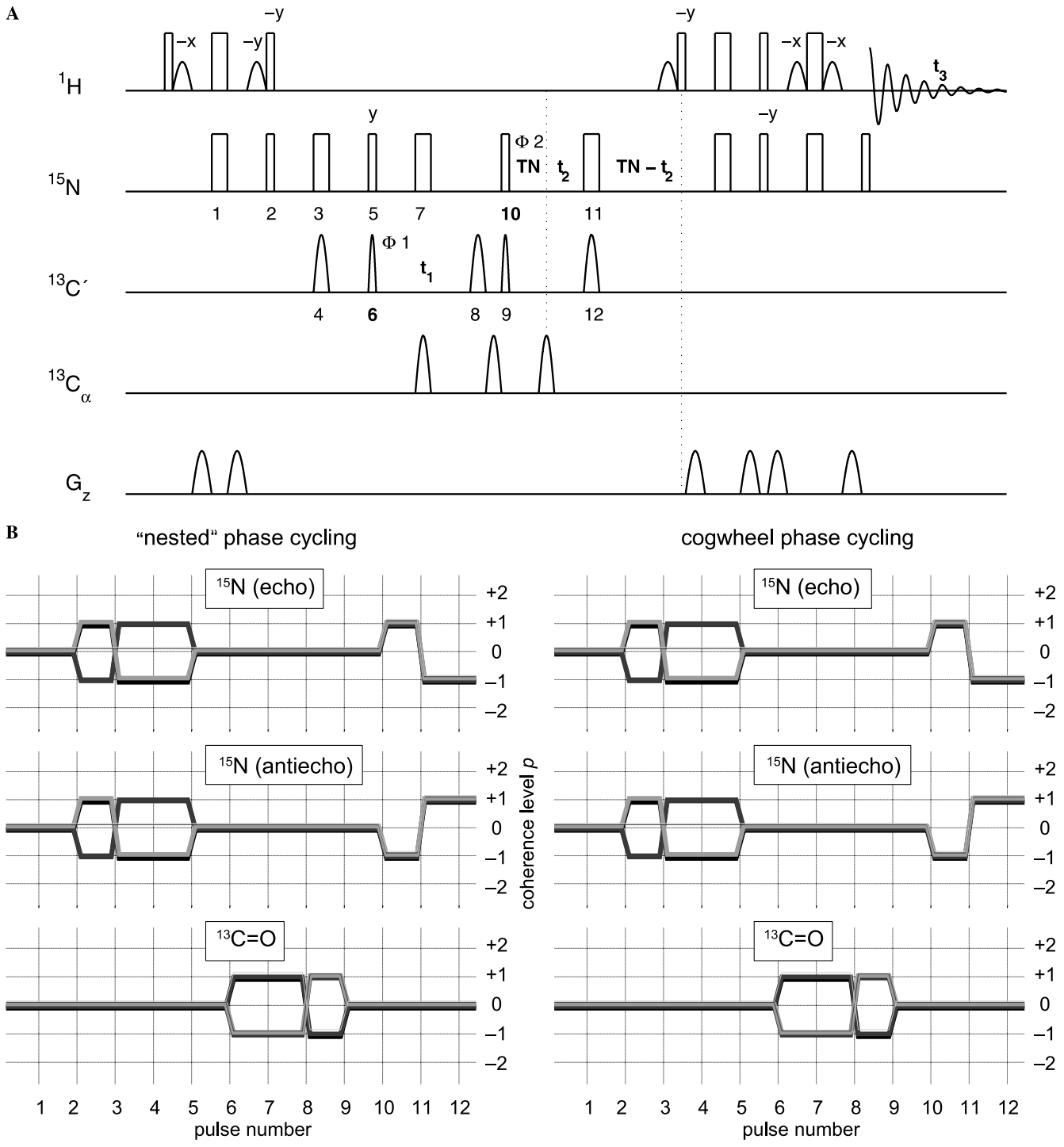

Fig. 1. TROSY-HNCO pulse sequence [23] (A) with coherence transfer diagrams simulated by CCCP [24] (B). The pulse sequence (A) is drawn as supplied with the instrument software [26]. In all displayed pulse sequences narrow and wide bars denote 90° and 180° rf-pulses. Arcs represent shaped 90° or 180° rf-pulses and pulsed field gradients (on G_Z). For cPC coherence selection of A we cycled the phases of the same pulses as in the nPC experiment, labelled here as pulses 6 (Φ_1) and 10 (Φ_2). The upper and lower ^{15}N channel coherence pathway diagrams differ in the cycling of pulse 10 and correspond to COG*6*(3,1;2) and COG*6*(3,5;2) cPCs, respectively, which are used to achieve quadrature detection by the echo/anti-echo protocol. Details of the phase cycles are given in Table 1. The bottom ^{13}C=O coherence pathway diagram is identical in both cases. The simulations take an error of −5% in the 90° pulse flip angles into account. Note, that the thin lines in the diagrams reflect the breakthrough of unwanted coherences. In all cases shown the most intense of these pathways have less than 3% of the amplitude of the main desired pathways drawn with bold lines and are equal for cPC and nPC selection.

schemes used. The CTPs selected by the cPC COG*6*(3,1;2) and the 8-step nPC (echo) presented in Fig. 1B were compared on the basis of the selection rules established by Levitt et al. [14] and Bodenhausen et al. [16]. A CTP vector $P = (p_6^-, p_6^+, p_{10}^-, p_{10}^+)$ represents the coherence orders before (−) and after (+) the pulses 6

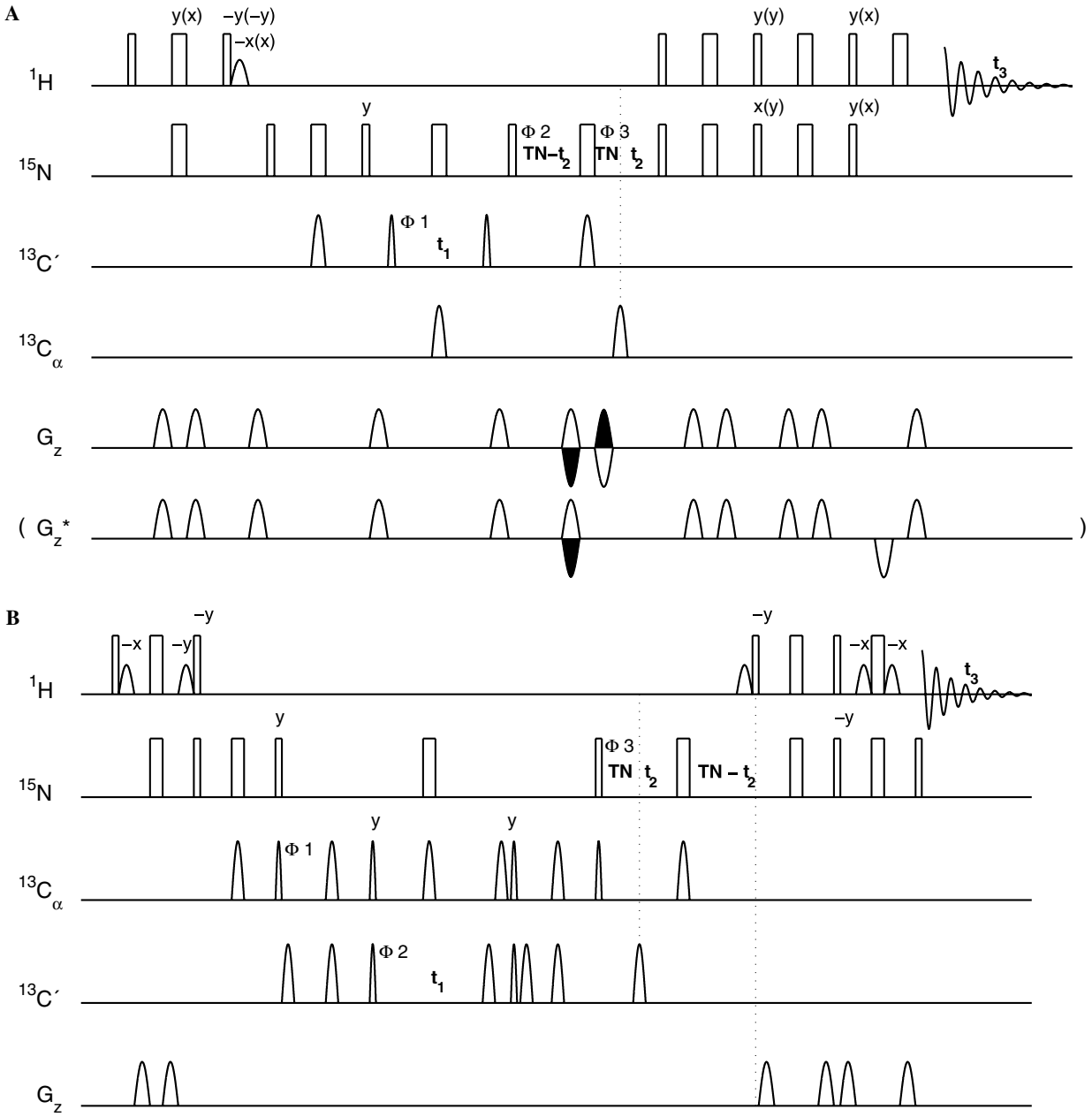

Fig. 2. Sensitivity-enhanced TROSY-HNCO [32] and TROSY-HN(CA)CO [27] experiment. Both experiments use equal phase cycling schemes, similar to that employed in the above presented TROSY-HNCO [23] (Fig. 1A). For implementation on a Bruker DRX spectrometer experiment (A) was modified from its original version in Ref. [32] in the following way: Proton and nitrogen pulse phases were set according to the labels on top of the pulses. Labels in brackets denote original phase settings from Ref. [32]. Gradients displayed on G_Z were used instead of the bracketed original gradients on G_Z^* from Ref. [32]. Black and white gradients of opposite sign indicate echo/anti-echo selection in the corresponding indirect dimension [34].

Table 1
Phase cycling scheme[a] for TROSY-HNCO with nPC and cPC[b]

"Nested" phase cycling 8 steps									Cogwheel phase cycling 6 steps COG6 (3,1/5;2)						
Step	1	2	3	4	5	6	7	8	Step	1	2	3	4	5	6
Φ_1	0°	0°	0°	0°	180°	180°	180°	180°	Φ_1	0°	180°	0°	180°	0°	180°
Φ_2 (echo)	90°	270°	0°	180°	90°	270°	0°	180°	Φ_2 (echo)	0°	60°	120°	180°	240°	300°
Φ_2 (anti-echo)	90°	270°	180°	0°	90°	270°	180°	0°	Φ_2 (anti-echo)	0°	300°	240°	180°	120°	60°
Φ_{rec}	90°	270°	180°	0°	270°	90°	0°	180°	Φ_{rec}	0°	120°	240°	0°	120°	240°

[a] All pulse phases of the phase cycling procedure are given in degrees and refer to Fig. 1.
[b] v_1 is the winding number for pulse 6 and v_2 is the winding number for pulse 10. v_{rec} determines the phase cycling of the receiver phase Φ_{rec}. The actual phases during the cPC are derived from Eq. (2) in the theory section.

Table 2
Experimental SNR[a] for TROSY-HNCO/-HN(CA)CO and HACACO employing nPCs and cPCs[b]

Phase cycling	NS	SNR normalized
TROSY-HNCO		
NEST*8* (2 × 4)	8	1,00
COG*4*(2,1/3;1)	4	1,07
COG*6*(3,2/4;1)	6	1,04
TROSY-HN(CA)CO		
NEST*8* (2 × 4)	8	1,00
COG*4*(2,1/3;1)	4	0,94
COG*6*(3,2/4;1)	6	1,03
HACACO		
NEST*16* (2 × 2 × 2 × 2)	16	1,00
COG*3* (0,0,2/1,2/1;1)	3	1,16
COG*4*(2,2,3/1,3/1;2)	4	1,00
COG*5*(1,4,3,4;2)	5	0,57
COG*6*(3,3,4/2,1/5;5)	6	1,06
COG*7*(0,0,2/5,2/5;4)	7	1,04
COG*8*(4,4,5/3,1/7;6)	8	1,04

[a] SNR normalized gives the average values determined from 10 peaks in each first $^{1}H/^{13}CO$, $^{1}H/^{13}C_{\alpha}$ or $^{1}H/^{15}N$ plane in the respective 3D experiments. NS is the number of scans.

[b] In all cPC modified experiments only the same pulses as in the nPC pulse sequence are cycled. Winding numbers v_1 and v_2 in the TROSY-HNCO experiment affect pulses 6 and 10 in Fig. 1. The phase cycling scheme for TROSY-HN(CA)CO is analogous. In the HACACO (Fig. 2) experiment v_1 cycles pulse 2, v_2 cycles pulse 7, v_3 cycles pulse 11 and v_4 cycles pulse 16.

and 10 (Fig. 1A). The two desired CTP vectors form the vector set $P = \{(0, \pm1, 0, 1)\}$. The cPC selects the following CTP vector sets in addition to the ones selected by the nPC: $P_2 = \{(\pm2, \pm2|0, 1, -1)\}$, $P_1 = \{(\pm1, \pm1, 1, -1)\}$, and $P_0 = \{(0, \pm2|0, 1, -1)\}$. The vector groups P_2 and P_1 do not fulfill the initial condition of pure z-magnetization before the first pulse and can therefore be neglected unless repetition rates are very fast compared to T_2. Also, assuming that the first 90° pulse on any channel can only create ±1 QC, two out of three vectors in P_0 are excluded. Only $P = \{(0, 0, 1, -1)\}$, with 1QC before pulse 10, is a priori an interfering pathway arising due to the use of COG*6*(3,1;2) instead of the original nested phase cycle. CCCP calculations, however, give no significant amplitude for this CTP. COG*4*(2,1/3;1) represents another suitable and experimentally tested cPC (see Table 2). To cycle the same three pulses as in the pulse sequence described by Yang and Kay, the use of e.g. COG*6*(3,3,1/5;2) is recommended. This cPC yields virtually identical coherence transfer diagrams as compared to the experiment employing nPC.

The results obtained for the TROSY-HNCO experiment are directly transferable to pulse sequences using analogous phase cycling schemes, like the TROSY-HNCA [23] and TROSY-HN(CA)CO experiments [27]. The latter experiment as shown in Fig. 2B is implemented in the Bruker library [26] using an eight step nPC and also PFGs. Since also in this case the phase cycling is only affecting one $^{13}C{=}O$ and one ^{15}N pulse the same approach as presented for the TROSY-HNCO experiment above can be used.

An additional two-step phase cycle may be imposed on the first 90° pulse of the INEPT transfer step from $^{13}C_{\alpha}$ to $^{13}C{=}O$, to better suppress axial peak artefacts resulting in a minimum of 16 scans in the nPC version of the experiment. Adding this phase cycle in a nested fashion to the proposed COG*4* and COG*6* phase cycles yields 8 and 12 totally required scans, respectively. CCCP++ searches for pure cPCs, which cycle all three pulses yielded COG*4* and COG*6* cPCs, e.g. COG*4*(2,2,1/3;3) and COG*6*(3,3,1/5;1), which select all parallel pathways and show equal selection properties to the 16 step nPC. Both cPC examples fulfil the above proposed design rule for cPCs retaining parallel coherence pathways. In this case the cycling of one additional 90° pulse in a nested fashion doubles the totally required number of scans, while the same coherence selection is also achievable with COG*4* and COG*6* cPC.

4.2. HACACO

The HACACO (Fig. 3A) pulse sequence [31], again as supplied with the spectrometer software [26] uses a 16-step nested phase cycle. The nPC cycles four pulses in two steps each, thus allowing all possible parallel pathways. We determined and investigated cogwheel phase cycles of three to eight steps for this experiment. With the exception of the five-step cPCs we found that the cPC coherence selection allows one to maintain parallel pathways, while adequately suppressing undesired coherences. Like in the cases presented above, only the same pulses as in the original nPC experiment are phase cycled. The cPCs proposed and tested for HACACO are shown in Table 2. All CCCP simulations (Fig. 3B) show well-matching coherence transfer diagrams for the cPC schemes with respect to the corresponding nPC scheme. In the case of the cPC-modified HACACO experiment coherence selection during evolution times is achieved by combining PFGs and cPC. Echo-/anti-echo selection is performed with gradients, while the cycling of the preceding pulse 12 (Fig. 3A) allows parallel CTPs analogous to the nPC experiment.

It should be noted that in all above pulse sequences one may either decide to cycle only the pulses that are cycled in the original ''nested'' sequence, or rather cycle more pulses. According to our preliminary calculations, while increasing the number of cycled pulses tends to decrease the minimum required number of scans N, at the same time retention of parallel pathways becomes less likely.

5. Experimental results

TROSY-HNCO measurements on a sample of >99% ^{13}C and ^{15}N labelled ubiquitin employing cogwheel phase cycles (cPC) yield excellent spectra (Figs. 4 and 5) with no loss in per-scan signal-amplitude for four and six scans per transient. Only minor differences in signal-amplitude and spectral quality are observed upon switching between the two analyzed TROSY-HNCO pulse sequences [22,32] displayed in Figs. 1A and 2A. Cogwheel phase cycles are

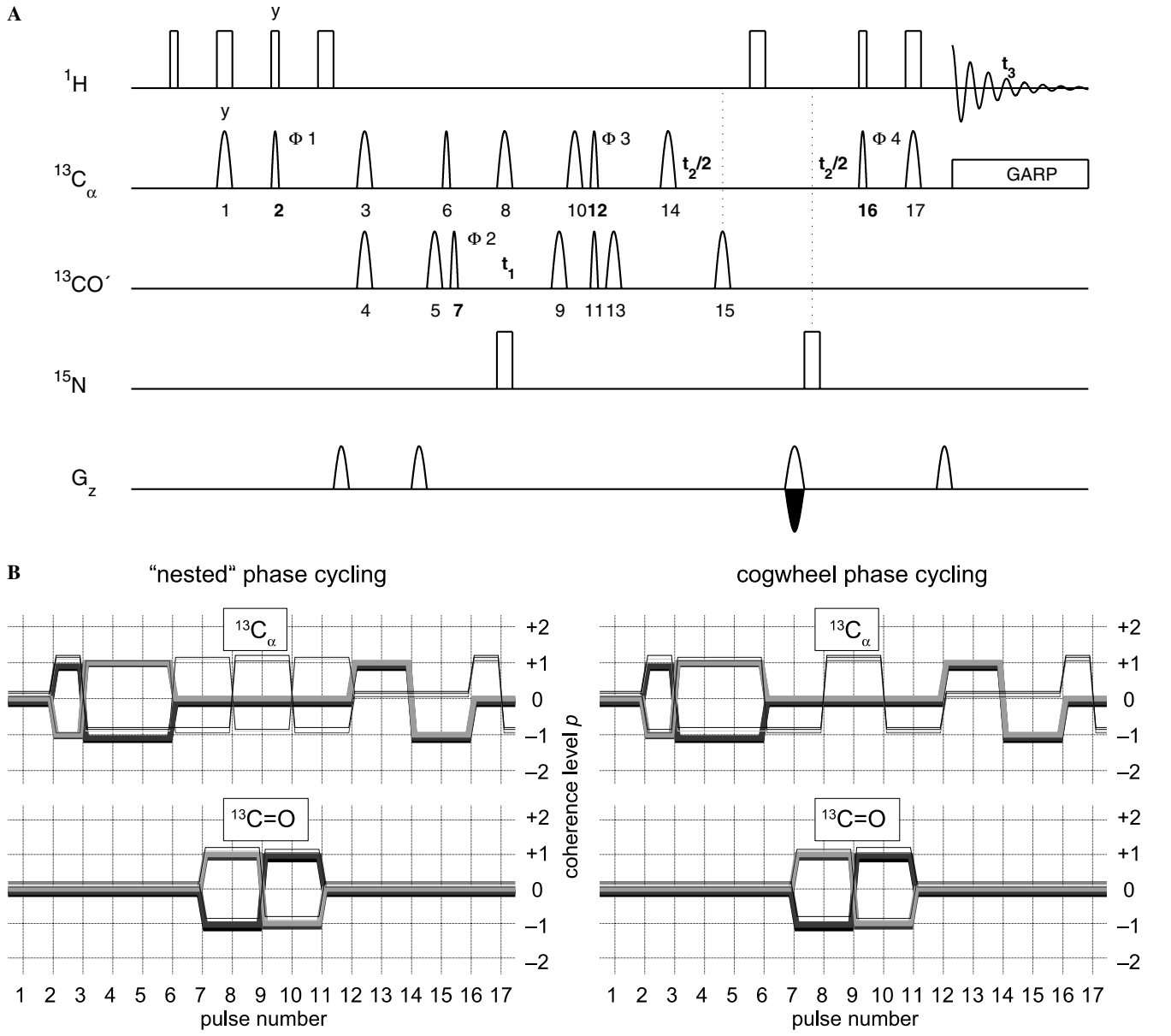

Fig. 3. HACACO pulse sequence [31] (A) and coherence transfer diagrams obtained by CCCP [24] (B). The pulse sequence is drawn as supplied by Bruker [26]. The alternating sign gradient affords echo/anti-echo selection in the t_2 ($^{13}C_\alpha$) evolution time. Note, that only the echo-path is displayed. All cPCs cycle again only the same pulses as the nPC. The cycled pulses are labeled with numbers 2 (Φ_1), 7 (Φ_2), 11 (Φ_3), and 16 (Φ_4), respectively (A). The coherence transfer diagram (B) displays the CCCP simulation results for the 16-step nPC cycling four pulses in two steps each and the 4-step cPC COG*4*(2,2,3,3;2) (echo). For the simulations an error of −5% in the 90° pulse flip angles was introduced. The thin lines in the diagrams reflect the most intense leakage pathways of undesired coherences. In both diagrams shown for nPC and cPC the most intense of these pathways have 9% of the amplitude of the main desired pathways drawn with bold lines.

equally well-suited to replace nested phase cycles in both cases. In Table 2 we compare a "normalized" SNR calculated as the signal to noise ratio over the square root of the number of transients, relative to the normalized SNR of the nested phase cycle. All given values correspond to an average of 10 peaks in the first 2D ^{1}H/^{15}N plane of a 3D TROSY-HNCO [23] experiment. Artefact suppression is well comparable with the "nested" (nPC) 8-step (2×4) version of the experiment. 2D ^{1}H/^{15}N planes from the unmodified "nested"- and the COG*6*(3,1/5;2) cPC-based gradient-enhanced 3D TROSY-HNCO experiment discussed in the previous Section are displayed in Figs. 4A and B. Echo- and anti-echo-pathway selection and TROSY enhancement work as expected from our simulations (Fig. 1B) and we are obtaining pure phase and equally good line shapes in both experiments. The comparison of signal intensities as average of 10 signals in the two spectra yield a ratio of 8.0 : 6.0 in accordance with the ratio of the numbers of accumulated transients (Fig. 4C and 3D). The first 2D ^{1}H/^{13}C=O planes of the corresponding nPC and cPC COG*4*(2,1/3;1) and COG*6*(3,2/4;1) experiments are compared in Fig. 5. All spectra are of comparable quality

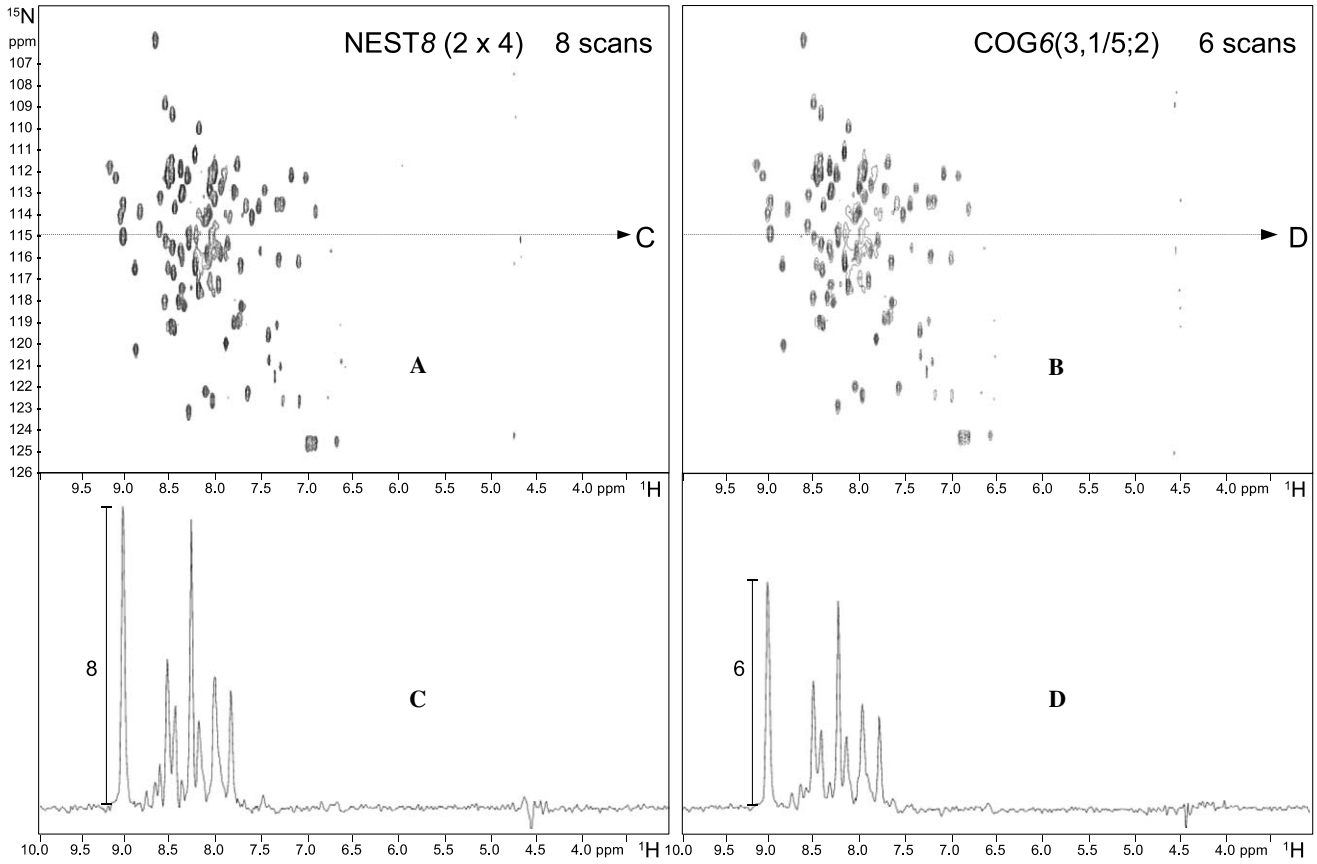

Fig. 4. TROSY-HNCO spectra recorded with nPC and cPC. Above, the first $^{1}H/^{15}N$ planes of 3D-TROSY-HNCO spectra of doubly (^{13}C and ^{15}N) labelled ubiquitin in H_2O/D_2O (90/10) recorded with pulse sequences employing 8-step nPC (A) and 6-step cPC COG*6* (3,1/5;2) (B) are shown. The ^{1}H 1D plots below (C and D) are taken from the same rows at 114,76 ppm ^{15}N chemical shift and are drawn to scale. The signals in the 1D plots show an intensity ratio of 8 (nested) : 6 (cogwheel). All spectra have been recorded on a 500 MHz Bruker DRX spectrometer, equipped with a cryogenically cooled triple resonance (TXI) probe. The same phase cycling procedure has also been tested successfully on a paramagnetic aquo-myoglobin sample in the same solvent.

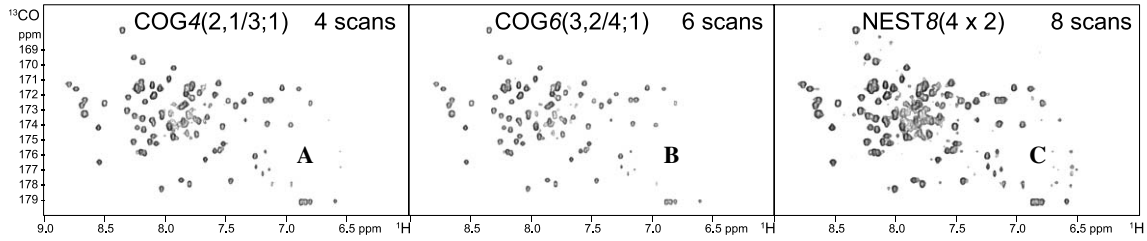

Fig. 5. Comparison of 2D $^{1}H/^{13}CO$ planes from TROSY-HNCO. TROSY-HNCO 2D $^{1}H/^{13}CO$ slices from cPC-based (COG*4*(1/3,2;1) (A) and COG*6*(2/4,3;1) (B)) experiments on double-labelled ubiquitin (Spectra Stable Isotopes) in H_2O/D_2O (90/10) are compared to the nPC 8-step version (C) of the experiment.

with respect to artefact suppression, normalized signal-to-noise ratios (Table 2), line shape, phase and presence of all expected peaks.

TROSY-HN(CA)CO experiments [27] require a minimum of eight scans for sufficient coherence selection in the gradient enhanced nPC version. We have tested the same cPCs as in the above discussed TROSY-HNCO experiment and obtained high quality spectra with only four and six scans per increment. Artefact suppression was good in all presented cases. Using 16 step nPC instead of the 8 step nPC and the corresponding COG*4*(2,2,1/3;3) and COG*6* (3,3,1/5;1) cPC discussed above did not noticeably improve the spectral quality. Furthermore it is noteworthy, that experiments employing COG*4*(2,1/3;1) suffered from small axial peak artefacts, which were not present in the COG*6*(3,2/4;1) cPC experiment, which therefore seems to be the most favorable coherence selection scheme for this experiment.

In a number of gradient enhanced HACACO [31] experiments on a paramagnetic cyano-metmyoglobin sample [32] in D_2O cPCs with three, four, five, six, seven, and eight steps have been compared with the 16-step ($2 \times 2 \times 2 \times 2$)

nPC (Fig. 3A). Our simulations (see Fig. 3B) show that most of the tested cPC phase cycling procedures can select all desired parallel CTPs cycling the same four pulses. Therefore, we obtain similar normalized signal-to-noise ratios for these experiments as with nPC (see Table 2). For cPCs which cannot select parallel pathways in one coherence transfer step, as for the case of five-step cPC, we obtain only half of the intensity. The number of allowed coherence transfer pathways calculated by CCCP++ matches the experimental results. All displayed cPC enhanced experiments yield spectra with good artefact suppression, comparable normalized SNR and show all expected resonances when checked against the nPC result.

6. Discussion and conclusions

By simultaneous instead of independent incrementation of pulse phases, cogwheel phase cycling efficiently reduces the minimum required number of scans also in liquid-state triple resonance NMR pulse sequences commonly used for protein assignment and structure elucidation. We have investigated the theoretical and practical performance of cPC modified 3D NMR triple resonance pulse sequences: In TROSY-HNCO and TROSY-HN(CA)CO only four cogwheel steps can achieve a comparable coherence selectivity as an eight steps ''nested'' phase cycle. This corresponds to a 50% reduction in total recording time. Even more impressive gains in efficiency are possible for selected experiments like the HACACO experiment. COG*3* cPCs achieves the coherence selection in a quality comparably to 16 step nPCs, which corresponds to more than 80% time saving. Since the presented cPC-enhanced experiments cycle only the same pulses as the corresponding nPC versions, existing pulse programs can be easily modified. Simultaneous phase cycling of more pulses allows one to select a single desired coherence pathway in a minimum number of steps. However, usually the selection of parallel coherence pathways is desired to obtain maximum per-scan sensitivity. To achieve this cycling only a well selected minimum number of pulses appears advisable.

Cogwheel phase cycles for a densely spaced series of scan numbers N with similar practical performance were found for all experiments discussed. The possibility to vary the number of accumulated transients in small steps allows for greatly enhanced flexibility in adjusting the total number of scans to the desired signal-amplitude. The restrictions of using multiples of the minimum nested phase cycle steps are hence released.

Today most commonly used pulse sequences use both, pulsed field gradients and ''nested'' phase cycles for efficient coherence selection. We have demonstrated that combining cogwheel phase cycling with pulsed field gradients is easily implemented and results in significantly shorter total experiment duration. At the same time artefact suppression comparable to conventional phase cycled experiments is achieved. We also showed that it is possible to find short coherence selection schemes using cogwheel phase cycles which allow for parallel coherence pathways thus causing no per scan signal loss.

Using cogwheel phase cycles for coherence selection in high resolution liquid state multi-pulse NMR experiments helps to fully exploit the advantages of modern NMR hardware, in particular the sensitivity gains offered by cryogenically cooled probes.

Acknowledgments

We are very grateful to Malcolm H. Levitt for helpful comments on an early version of the manuscript. The authors thank Dr. Wolfgang Bermel for his continued support in pulse programming. This work has been supported by the Austrian Science Fund (FWF) Project P15380.

References

[1] P. Styles, N.F. Soffe, C.A. Scott, D.A. Crag, F. Row, D.J. White, P.C.J. White, A high-resolution NMR probe in which the coil and preamplifier are cooled with liquid helium, J. Magn. Reson. 60 (1984) 397–404.
[2] M. Jerosch-Herold, R.K. Kirschman, Potential benefits of a cryogenically cooled nmr probe for room-temperature samples, J. Magn. Reson. 85 (1989) 141–146.
[3] L. Frydman, T. Scherf, A. Lupulescu, The acquisition of multidimensional NMR spectra within a single scan, Proc. Natl. Acad. Sci. USA 99 (25) (2002) 15858–15862.
[4] L. Frydman, A. Lupulescu, T. Scherf, Principles and features of single-scan two-dimensional NMR spectroscopy, J. Am. Chem. Soc. 125 (2003) 9204–9217.
[5] Y. Shrot, L. Frydman, Single-scan NMR spectroscopy at arbitrary dimensions, J. Am. Chem. Soc. 125 (2003) 11385–11396.
[6] S. Mori, C. Abeygunawardana, M.O. Johnson, P.C.M. Vanzijl, Improved sensitivity of HSQC spectra of exchanging protons at short interscan delays using a new fast HSQC (FHSQC) detection scheme that avoids water saturation, J. Magn. Reson. 109 (1995) 94–98.
[7] T. Szyperski, G. Wider, J.H. Bushweller, K. Wüthrich, Reduced dimensionality in triple-resonance NMR experiments, J. Am. Chem. Soc. 115 (1993) 9307–9308.
[8] T. Szyperski, D.C. Yeh, D.K. Sukumaran, H.N.B. Moseley, G.T. Montelione, Reduced-dimensionality NMR spectroscopy for high-throughput protein resonance assignment, Proc. Natl. Acad. Sci. USA 99 (12) (2002) 8009–8014.
[9] E. Kupče, R. Freeman, Reconstruction of the three-dimensional NMR spectrum of a protein from a set of plane projections, J. Biomol. NMR 27 (2003) 383–387.
[10] E. Kupče, R. Freeman, Projection–reconstruction of three-dimensional NMR spectra, J. Am. Chem. Soc. 125 (2003) 13958–13959.
[11] E. Kupče, R. Freeman, Projection–reconstruction technique for speeding up multidimensional NMR spectroscopy, J. Am. Chem. Soc. 126 (2004) 6429–6440.
[12] L. McIntyre, R. Freeman, Fast two-dimensional correlation spectroscopy, J. Magn. Reson. 83 (1989) 649–655.
[13] C.E. Hughes, M. Carravetta, M.H. Levitt, Some conjectures for cogwheel phase cycling, J. Magn. Reson. 167 (2004) 259–265.
[14] M.H. Levitt, P.K. Madhu, C.E. Hughes, Cogwheel phase cycling, J. Magn. Reson. 155 (2002) 300–306.
[15] N. Ivchenko, C.E. Hughes, M.H. Levitt, Application of cogwheel phase cycling to sideband manipulation experiments in solid-state NMR, J. Magn. Reson. 164 (2003) 286–293.

[16] G. Bodenhausen, H. Kogler, R.R. Ernst, Selection of coherence-transfer pathways in NMR pulse experiments, J. Magn. Reson. 58 (1984) 370–388.
[17] A.D. Bain, Coherence levels and coherence pathways in NMR. A simple way to design phase cycling procedures, J. Magn. Reson. 56 (1984) 418–427.
[18] A. Bax, P.G. De Jong, A.F. Mehlkopf, J. Smidt, Separation of the different orders of NMR multiple-quantum transitions by the use of pulsed field gradients, Chem. Phys. Lett. 69 (3) (1980) 567–570.
[19] J. Keeler, R.T. Clowes, A.L. Davis, E.D. Laue, Pulsed-field gradients: theory and practice, Methods Enzymol. 239 (1994) 145–207.
[20] C.J.R. Counsell, M.H. Levitt, R.R. Ernst, The selection of coherence-transfer pathways by inhomogeneous z pulses, J. Magn. Reson. 64 (1985) 470–478.
[21] I. Bertini, C. Luchinat, G. Parigi, Solution NMR of Paramagnetic Molecules, Current Methods in Inorganic Chemistry, Elsevier, Amsterdam, 2001.
[22] I. Bertini, C. Luchinat, G. Parigi, R. Pierattelli, NMR spectroscopy of paramagnetic metalloproteins, Chem. Biol. Chem. 6 (9) (2005) 1536–1549.
[23] M. Salzmann, K. Pervushin, G. Wider, H. Senn, K. Wüthrich, TROSY in triple-resonance experiments: new perspectives for sequential NMR assignment of large proteins, Proc. Natl. Acad. Sci. USA 95 (1998) 13585–13590.
[24] A. Jerschow, N. Müeller, Efficient simulation of coherence transfer pathway selection by phase cycling and pulsed field gradients in NMR, J. Magn. Reson. 134 (1998) 17–29.
[25] A. Jerschow, R. Kumar, Calculation of coherence pathway selection and cogwheel cycles, J. Magn. Reson. 160 (2003) 59–64.
[26] NMR-Suite 3.5 patchlevel 6, Bruker Biospin, Rheinstetten (2003).
[27] M. Salzmann, G. Wider, K. Pervushin, H. Senn, K. Wüthrich, TROSY-type triple-resonance experiments for sequential NMR assignments of large proteins, J. Am. Chem. Soc. 121 (1999) 844–848.
[28] M. Piotto, V. Saudek, V. Sklenář, Gradient-tailored excitation for single-quantum NMR spectroscopy of aqueous solutions, J. Biomol. NMR 2 (1992) 661–665.
[29] L.E. Kay, P. Keifer, T. Saarinen, Pure absorption gradient enhanced heteronuclear single quantum correlation spectroscopy with improved sensitivity, J. Am. Chem. Soc. 114 (1992) 10663–10665.
[30] D. Marion, M. Ikura, R. Tschudin, A. Bax, Rapid recording of 2D NMR spectra without phase cycling. Application to the study of hydrogen exchange in proteins, J. Magn. Reson. 85 (1989) 393–399.
[31] L.E. Kay, M. Ikura, R. Tschudin, A. Bax, Three-dimensional triple-resonance NMR spectroscopy of isotopically enriched proteins, J. Magn. Reson 89 (1990) 496–514.
[32] G. Pintacuda, K. Hohenthanner, G. Otting, N. Müller, Angular dependence of dipole–dipole–Curie–spin cross-correlation effects in high-spin and low-spin paramagnetic myoglobin, J. Biomol. NMR 27 (2003) 115–132.
[33] D. Yang, L.E. Kay, Improved ^{1}HN-detected triple resonance TROSY-based experiments, J. Biomol. NMR 13 (1999) 3–10.
[34] L.E. Kay, P. Keifer, T. Saarinen, Pure absorption gradient enhanced heteronuclear single quantum correlation spectroscopy with improved sensitivity, J. Am. Chem. Soc. 114 (1992) 10663–10665.